Journal of ELECTRONIC MATERIALS, Vol. 44, No. 1, 2015
DOI: 10.1007/s11664-014-3465-y

Characterization and Luminescence Properties of Color-Tunable Dy^{3+}-Doped BaY_2ZnO_5 Nanophosphors

SONIKA,[1] S.P. KHATKAR,[1] AVNI KHATKAR,[2] RAJESH KUMAR,[2] and V.B. TAXAK[1,3]

1.—Department of Chemistry, Maharshi Dayanand University, Rohtak 124001, India. 2.—U.I.E.T, Maharshi Dayanand University, Rohtak 124001, India. 3.—e-mail: v_taxak@yahoo.com

Dy^{3+}-doped BaY_2ZnO_5 nanophosphors were successfully synthesized by use of a solution combustion process. The effects of sintering temperature and dysprosium concentration on the structural and luminescence characteristics of the phosphors were investigated. X-ray diffraction (XRD) analysis confirmed the formation of pure orthorhombic BaY_2ZnO_5 with the space group *Pbnm* at 1100°C. Morphological investigation revealed spherical nanoparticles with smooth surfaces. The luminescence features of the nanophosphor were studied by use of photoluminescence excitation (PLE) and photoluminescence emission (PL), with luminescence decay curves and color (x, y) coordinates. On excitation at 355 nm, BaY_2ZnO_5 nanophosphor doped with trivalent dysprosium ion emits white light as a mixture of blue ($^4F_{9/2} \rightarrow {}^6H_{15/2}$) and yellow ($^4F_{9/2} \rightarrow {}^6H_{13/2}$) emission. Concentration quenching is explained on the basis of cross-relaxation between intermediate Dy^{3+} states. Thus, BaY_2ZnO_5:Dy^{3+} nanophosphor may be suitable for producing efficient white light for ultraviolet-light-emitting diodes (UV-LEDs), fluorescent lamps, and a variety of optical display panels.

Key words: Nanophosphor, solution combustion process, white light, BaY_2ZnO_5:Dy^{3+}

INTRODUCTION

During the last decade, rare earth-based nanophosphors have been at the forefront of scientific research because of their unique electronic, optical, and chemical properties, arising from the 4*f* shell, and their significant applications in opto-electronics devices, solid-state lighting, photonics, field emission displays, luminescent paints, cathode rays tubes, light-emitting diodes, biological labeling, lasers, and fluorescent lamps, among others.[1–5] The luminescence of these nanomaterials is highly dependent on the interaction of rare earth ions (RE^{3+}) with the host crystalline structure, local symmetry, structural disorder, the ability of the crystal lattice to host RE^{3+}, dopant concentration, and efficient energy transfer between host and dopant ions.[6] Apart from their excellent magnetic, thermal, electronic, and superconducting properties, the ternary oxides $BaLn_2ZnO_5$ (Ln = trivalent lanthanide ions) with stable crystal structure have, when doped with different RE^{3+} ions, emerged as potential luminescent materials.[7–23] $BaLn_2ZnO_5$ compounds containing Sm, Eu, Gd, Dy, Ho, Y, Er, or Tm ions have an orthorhombic structure belonging to space group *Pbnm*; those containing the La or Nd ions have a tetragonal structure with the 14/mcm space group. The orthorhombic BaY_2ZnO_5 structure with the space group *Pbnm* comprises BaO_{11}, YO_7, and ZnO_5 polyhedra.[24] In this lattice, Y^{3+} atoms occupy two different sevenfold oxygen-coordinated sites inside monocapped trigonal prisms having same crystal field symmetry (C_s) but slightly different Y–O distances. These prisms share edges to form wave-like chains parallel to the *b*-axis, and two such units join to form a basic Y_2O_{11} structure. Ba atoms reside in distorted elevenfold coordination

(Received May 9, 2014; accepted October 8, 2014; published online October 29, 2014)

cages whereas ZnO_5 has distorted tetragonal pyramidal coordination.[11–13]

Among RE^{3+} ions, trivalent dysprosium has been considered as a promising luminescent center for emission of white light originating from blue ($^4F_{9/2} \rightarrow {}^6H_{15/2}$) and yellow ($^4F_{9/2} \rightarrow {}^6H_{13/2}$) transitions.[25–28] From the perspective of efficient optoelectronic applications, nanophosphors with the desired composition, and reproducible size, shape, and structure, are essential; this can be achieved by use of reliable synthetic methods. To meet the requirement of white light emission, conventional efforts had been made to synthesize Dy^{3+}-doped $BaLn_2ZnO_5$ (Ln = Gd or Y) phosphor at high temperature.[11,12] In contrast with the vibrating milled solid-state method previously used for synthesis of BaY_2ZnO_5:Dy^{3+} phosphor, which requires sintering of 12 h at high temperature, i.e. 1250°C, solution combustion synthesis (SCS) has been introduced as a simple, low-cost, rapid, simple, and relatively green technique for preparation of phosphors of defined size and morphology, with fewer defects and excellent luminescence properties.[29] We have recently used SCS for synthesis of Eu^{3+}/Tb^{3+}-doped BaY_2ZnO_5 nanophosphors and have investigated their luminescence properties.[18,22] Because a search of the literature revealed that no work has been conducted on preparation of BaY_2ZnO_5:Dy^{3+} phosphors by use of SCS, in this study we synthesized a Dy^{3+}-doped BaY_2ZnO_5 nanophosphor by solution combustion. The dependence on dysprosium ion content of phase formation and tuning of the color of white emission for the single-phase host lattice were also investigated in detail.

EXPERIMENTAL

Powder Synthesis

$BaY_{2(1-x)}ZnO_5$:$2xDy^{3+}$ nanophosphors were synthesized by a solution combustion approach from high-purity $Ba(NO_3)_2$, $Y(NO_3)_3{\cdot}6H_2O$, $Zn(NO_3)_2$, $Dy(NO_3)_3{\cdot}6H_2O$, and urea as starting materials. The chemical reaction was:

$$Ba(NO_3)_2 + 2(1-x)Y(NO_3)_3 + 2xDy(NO_3)_3 + Zn(NO_3)_2 + 8.32CH_4N_2O\ (\text{urea}) \rightarrow BaY_{2(1-x)}Dy_{2x}ZnO_5(s) + \text{gaseous products.} \quad (1)$$

On the basis of the nominal composition $BaY_{2(1-x)}Dy_{2x}ZnO_5$, where x = 0.5–7 mol.%, stoichiometric amounts of the metal nitrates were dissolved in a minimum quantity of deionized water and then urea was added as fuel. The amount of urea was calculated on the basis of total oxidizing and reducing valencies of the oxidizer and the fuel (urea) according to the concept used in propellant chemistry.[30] This aqueous paste containing the calculated amounts of metal nitrates and urea was then placed in a preheated furnace maintained at 500°C. The mixture of metal nitrates (oxidizers) and fuel (urea) underwent rapid and self-sustaining combustion, and the chemical energy released during the exothermic redox reaction resulted in dehydration and foaming followed by decomposition. Consequently, large amounts of volatile combustible gases were generated, with flames, yielding a voluminous solid within 5–8 min. SCS utilizes the enthalpy of combustion for formation of $BaY_{2(1-x)}$-$Dy_{2x}ZnO_5$ nanophosphors. The powders obtained were sintered at different temperatures for 3 h to investigate the effect of sintering on the structural and luminescence features of BaY_2ZnO_5:Dy^{3+} nanophosphor.

Powder Characterization Techniques

The phase purity of $BaY_{2(1-x)}ZnO_5$:$2xDy^{3+}$ powders was evaluated by x-ray diffraction (XRD) using a Rigaku Ultima IV diffractometer with CuKα radiation, at a tube voltage of 40 kV and 40 mA tube current, in the 2θ range between 10° and 80°. The surface morphology of the samples was examined by use of a Jeol JSM-6510 scanning electron microscope (SEM). Photoluminescence excitation and emission in the ultraviolet–visible region and decay curves in the time-scan mode were studied, at room temperature, by use of an Hitachi F-7000 fluorescence spectrophotometer equipped with an Xe lamp. All measurements were performed in the Department of Chemistry, Maharshi Dayanand University, Rohtak, India. Crystallite size and shape were evaluated by transmission electron microscopy (TEM) with an Hitachi, Japan, H-7500 at the Sophisticated Analytical Instrumentation Facility (SAIF), Panjab University, Chandigarh, India.

RESULTS AND DISCUSSION

Crystal Structure and Particle Morphology

XRD profiles of $BaY_{1.92}Dy_{0.08}ZnO_5$ nanophosphor as-synthesized and after sintering at 800°C to 1100°C are compared with JCPDS standard no. 049-0516 in Fig. 1. As-synthesized $BaY_{1.92}Dy_{0.08}ZnO_5$ powder is poorly crystalline, as is apparent from relatively weak and broad peaks corresponding to the BaY_2ZnO_5 phase, in addition to many other peaks, denoted "*", arising from undecomposed nitrates in the sample. The powder sintered at 800°C contains the BaY_2O_4 (JCPDS no. 082-2319) and Y_2O_3 (JCPDS no. 088-2162) phases, labeled "■" and "•", respectively, with the BaY_2ZnO_5 phase. Even at 900°C, the pure orthorhombic phase could not be obtained, because the secondary BaY_2O_4 phase was still detected in the sample with all the characteristic BaY_2ZnO_5 peaks. At 1100°C, all the peaks in the diffraction patterns were well indexed to the dominant orthorhombic BaY_2ZnO_5 phase (JCPDS no. 049-0516, *Pbnm* space group, lattice parameters a = 7.070 Å, b = 12.33 Å and c = 5.709 Å). No traces

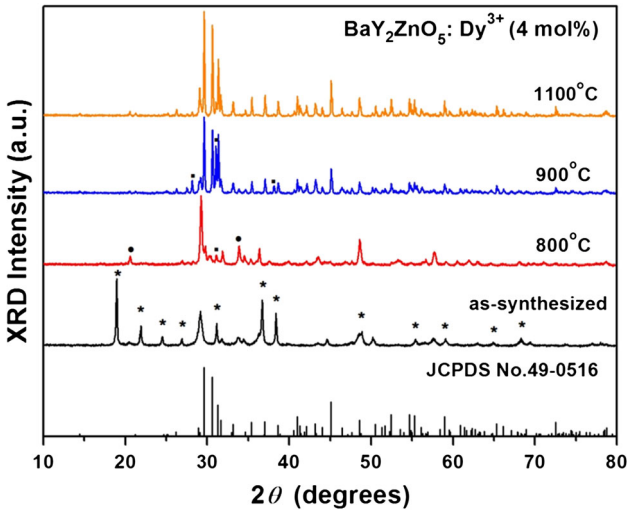

Fig. 1. XRD patterns of $BaY_{1.92}Dy_{0.08}ZnO_5$ nanophosphors as-synthesized and sintered at different temperatures, with JCPDS standard no. 049-0516.

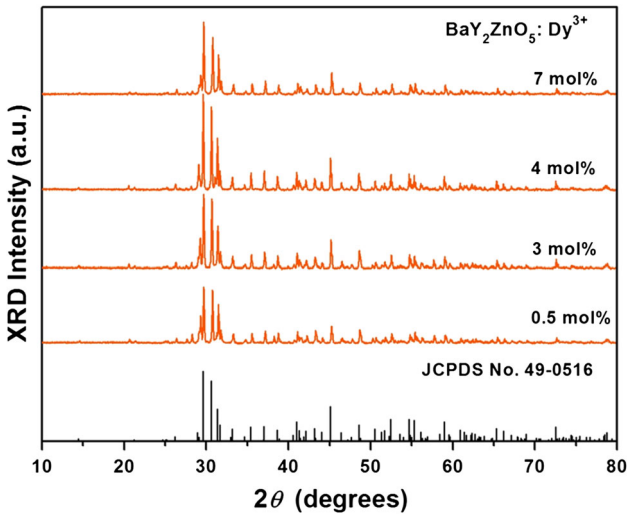

Fig. 2. XRD patterns of $BaY_{2(1-x)}Dy_{2x}ZnO_5$ powders sintered at 1100°C, doped with different contents of Dy^{3+} ions, with JCPDS standard no. 049-0516.

of other peaks from other phases apart from the single orthorhombic BaY_2ZnO_5 phase were observed at this temperature. It is clearly apparent that on increasing the temperature the intensity of main peak at 29.61° assigned to the (131) plane is enhanced, with a decrease in line width, indicating that the crystallinity of dysprosium-doped BaY_2ZnO_5 nanocrystals is improved by increasing the sintering temperature.

Figure 2 illustrates the XRD patterns of $BaY_{2(1-x)}Dy_{2x}ZnO_5$ powders sintered at 1100°C, doped with different amounts of dysprosium ions, with JCPDS standard no. 049-0516.

The closeness of the ionic radii of Y^{3+} (0.96 Å) and Dy^{3+} (0.97 Å) makes the substitution process easier at sites with the same symmetry (C_s) in the BaY_2ZnO_5 host lattice.[24] It is evident that all the samples have the single orthorhombic BaY_2ZnO_5 phase belonging to space group *Pbnm*, indicating that a small quantity of doped Dy^{3+} ions had no effect on the crystallographic structure of BaY_2ZnO_5. The crystallite size, D, of $BaY_{2(1-x)}ZnO_5$:$2x$-Dy^{3+} was estimated by use of Scherrer's formula:

$$D = 0.941\lambda/\beta\cos\theta \qquad (2)$$

where λ is the wavelength of CuKα radiation (0.1548 nm), β is the full width in radians at half-maximum (FWHM), and θ is the Bragg angle of an observed x-ray diffraction peak. The calculated average crystallite sizes (D) corresponding to the observed phases for different mol.% Dy^{3+} ions in $BaY_{2(1-x)}ZnO_5$ nanophosphors, sintered at different temperatures, are summarized in Table I. It was observed that all the powders are in the nano range, although an increase in crystallite size with increasing sintering temperature was noticed, because enhanced atomic mobility of particles leads to faster grain growth at higher temperature.

Figure 3 shows the SEM image of $BaY_{1.92}Dy_{0.08}ZnO_5$ powder sintered at 1100°C. Narrow size distribution of spherical particles, with slight agglomeration, are apparent. Uniform and smooth spherical morphology of $BaY_{1.92}Dy_{0.08}ZnO_5$ sintered at 1100°C in the diameter range 80–90 nm is also apparent from the TEM micrograph (Fig. 4). The high crystalline quality of the Dy^{3+}-doped BaY_2ZnO_5 nanoparticles indicated by XRD results has been confirmed by TEM, because crystallite size estimates from both analyses are consistent. Morphology studies revealed that $BaY_{1.92}Dy_{0.08}ZnO_5$ nanocrystalline particles are spherical. Because of high packing density, less light scattering, and brighter luminescence, these are more desirable than irregularly shaped particles because good crystallization substantially affects the photoluminescence properties.[31]

Luminescence Studies

The photoluminescence excitation (PLE) spectrum of $BaY_{1.92}Dy_{0.08}ZnO_5$ nanophosphor sintered at 1100°C, measured with λ_{em} = 580 nm, corresponding to the $^4F_{9/2} \rightarrow {}^6H_{13/2}$ transition in the 200–500 nm range, is shown in Fig. 5. The PLE spectrum consists of a broad band in the ultraviolet region (200–250 nm) with a maximum at 241 nm; this might arise as a result of overlapping of charge-transfer states (CTS), because of Dy^{3+} and O^{2-} interactions. The spectrum contains several sharp excitation lines originating from intra-configurational 4*f* transitions from the ground state $^6H_{15/2}$ to excited states of Dy^{3+} ions; the peak centered at ~355 nm ($^6H_{15/2} \rightarrow {}^4M_{15/2} + {}^6P_{7/2}$) is prominent.[13] The sharp excitation peaks observed in the range 250–500 nm for $BaY_{1.92}Dy_{0.08}ZnO_5$ nanophosphor, sintered at 1100°C, monitored with 580 nm as emission wavelength, are identified in Table II.

Table I. Crystallite size (nm), calculated by use of Scherrer's formula, for $BaY_{2(1-x)}ZnO_5$ nanophosphors containing different mol.% Dy^{3+} ions, sintered at different temperatures

	$BaY_{2(1-x)}Dy_{2x}ZnO_5$ phase and crystallite size (nm) after sintering at:							
	500°C		800°C		900°C		1100°C	
x = 0.5 mol.%	BaY_2ZnO_5	18.5	BaY_2ZnO_5	34.6	BaY_2ZnO_5	64.0	BaY_2ZnO_5	80.0
			BaY_2O_4	35.9	BaY_2O_4	76.8		
			Y_2O_3	36.5				
	$Ba(NO_3)_2$	53.2						
x = 3 mol.%	BaY_2ZnO_5	17.0	BaY_2ZnO_5	36.3	BaY_2ZnO_5	71.4	BaY_2ZnO_5	88.4
			BaY_2O_4	43.9	BaY_2O_4	78.2		
			Y_2O_3	35.5				
	$Ba(NO_3)_2$	75.3						
x = 4 mol.%	BaY_2ZnO_5	16.9	BaY_2ZnO_5	34.8	BaY_2ZnO_5	73.4	BaY_2ZnO_5	92.8
			BaY_2O_4	51.2	BaY_2O_4	82.8		
			Y_2O_3	37.9				
	$Ba(NO_3)_2$	66.1						
x = 7 mol.%	BaY_2ZnO_5	17.0	BaY_2ZnO_5	36.9	BaY_2ZnO_5	67.9	BaY_2ZnO_5	81.8
			BaY_2O_4	37.3	BaY_2O_4	71.2		
			Y_2O_3	32.9				
	$Ba(NO_3)_2$	55.6						

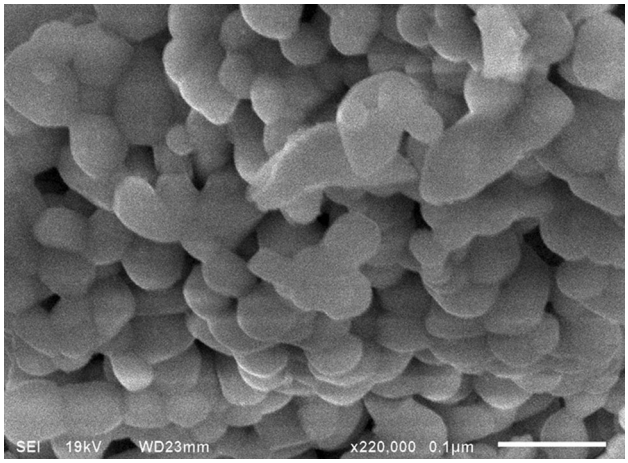

Fig. 3. SEM image of $BaY_{1.92}Dy_{0.08}ZnO_5$ nanophosphors sintered at 1100°C.

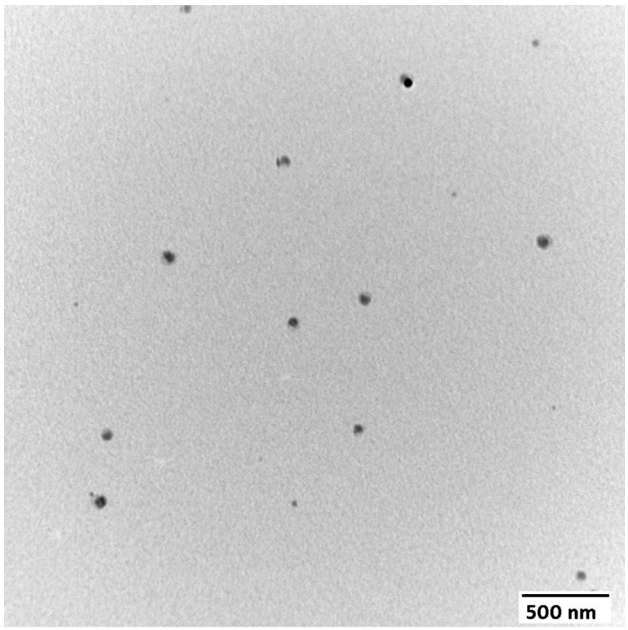

Fig. 4. TEM image of $BaY_{1.92}Dy_{0.08}ZnO_5$ nanophosphors sintered at 1100°C.

The photoluminescence (PL) spectra of $BaY_{1.92}Dy_{0.08}ZnO_5$ nanophosphors as-synthesized and sintered at different temperatures, measured in the range 400–650 nm with 355 nm as excitation wavelength, are shown in Fig. 6. The spectra comprise two main groups of lines in the blue 450–525 nm) and yellow (530–650 nm) regions. The blue emission peak at 490 nm and the yellow emission peak at 580 nm are assigned to the $^4F_{9/2} \rightarrow {}^6H_{15/2}$ and $^4F_{9/2} \rightarrow {}^6H_{13/2}$ transitions, respectively, of Dy^{3+} ions.[27] It is clearly apparent that the PL intensity of as-synthesized $BaY_{1.92}Dy_{0.08}ZnO_5$ nanophosphor corresponding to both blue and yellow transitions increases rapidly on increasing the sintering temperature from 800°C to 1100°C, as a result of reduction of non-radiative recombination effects, quenching sites, and surface defects in the crystal structure at higher temperature and, hence, better crystallinity.[2] In all $BaY_{1.92}Dy_{0.08}ZnO_5$ samples, the PL intensity of yellow emission ($^4F_{9/2} \rightarrow {}^6H_{13/2}$) was greater than that of blue emission ($^4F_{9/2} \rightarrow {}^6H_{15/2}$), because Dy^{3+} ions are located at non-inversion symmetry sites (C_s) in the BaY_2ZnO_5 lattice. This phenomenon occurs because the blue emission, which arises as a result of magnetic dipole transitions, is hardly affected by the

crystal field symmetry of Dy^{3+} ions whereas the yellow emission, which arises from hypersensitive forced electric transitions with the selection rule, $\Delta J = 2$, is strongly affected by the surroundings. The crystal field splitting of $^4F_{9/2} \rightarrow {}^6H_j$ can provide information about the site symmetry of Dy^{3+} ions with Kramer's doublets $(2J + 1)/2$ for each lattice site, where J is the angular momentum of the electrons.[32] In a host lattice, when Dy^{3+} ions occupy non-inversion symmetry sites, the yellow emission is stronger, whereas the blue transition dominates the emission spectrum when Dy^{3+} ions occupy high-symmetry local sites (with inversion centers). The photoluminescence features of nanophosphors confirm that Dy^{3+} ions are located at sevenfold Y^{3+} low-symmetry sites (C_s) in the BaY_2ZnO_5 lattice, as suggested by XRD studies.

PL spectra of $BaY_{2(1-x)}Dy_{2x}ZnO_5$ sintered at 1100°C as a function of dysprosium doping concentration, measured with 355 nm as excitation wavelength, are illustrated in Fig. 7. No distinct emission spectral features of $BaY_{2(1-x)}ZnO_5{:}2xDy^{3+}$ were observed on varying the x value from 0.5 mol.% to 7 mol.%, because the shape and positions remained the same. The emission spectra of all $BaY_{2(1-x)}Dy_{2x}ZnO_5$ samples contained characteristic both blue ($^4F_{9/2} \rightarrow {}^6H_{15/2}$) and yellow ($^4F_{9/2} \rightarrow {}^6H_{13/2}$) emission of Dy^{3+} ions, that from the hypersensitive ($^4F_{9/2} \rightarrow {}^6H_{13/2}$) transition being the stronger. The PL intensity of the $^4F_{9/2} \rightarrow {}^6H_J$ ($J = 15/2$ and $13/2$) transition of the nanophosphors was enhanced by increasing the doping concentration, and reached a maximum for $BaY_{2(1-x)}ZnO_5$ nanophosphor containing 4 mol.% Dy^{3+} ions. For 5 mol.% of dopant concentration, the emission intensity was reduced by a nominal value only, indicative of concentration quenching at higher dysprosium content. Cross relaxation among neighboring Dy^{3+} ions at higher concentrations is the most plausible explanation of such quenching behavior; this phenomenon depopulates the $^4F_{9/2}$ state of Dy^{3+} ions via non-radiative energy-transfer processes, i.e. Dy^{3+} ($^4F_{9/2}$) + Dy^{3+} ($^6H_{15/2}$) → Dy^{3+} ($^4F_{9/2}/{}^6H_{7/2}$) + Dy^{3+} ($^6F_{3/2}$).[33] Furthermore, the yellow-to-blue emission ratio (Y/B) is almost constant at 1.05 ± 0.02 over the range of Dy^{3+} content of BaY_2ZnO_5 nanophosphors. This leads to the assumption that the hypersensitive electric forced transition ($^4F_{9/2} \rightarrow {}^6H_{13/2}$) senses no substantial changes in the crystal field symmetry of Dy^{3+} sites in BaY_2ZnO_5 lattice at different doping concentrations.

The luminescence decay curves corresponding to the $^4F_{9/2} \rightarrow {}^6H_{13/2}$ emission line at 580 nm for

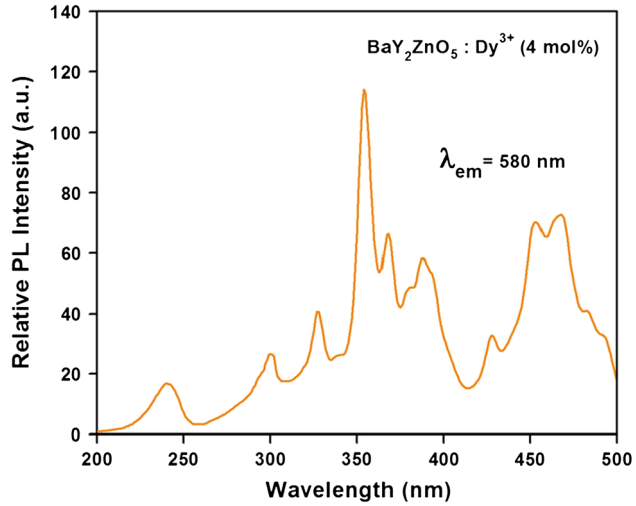

Fig. 5. Photoluminescence excitation (PLE) spectrum of $BaY_{1.92}Dy_{0.08}ZnO_5$ nanophosphor sintered at 1100°C, monitored with λ_{em} = 580 nm.

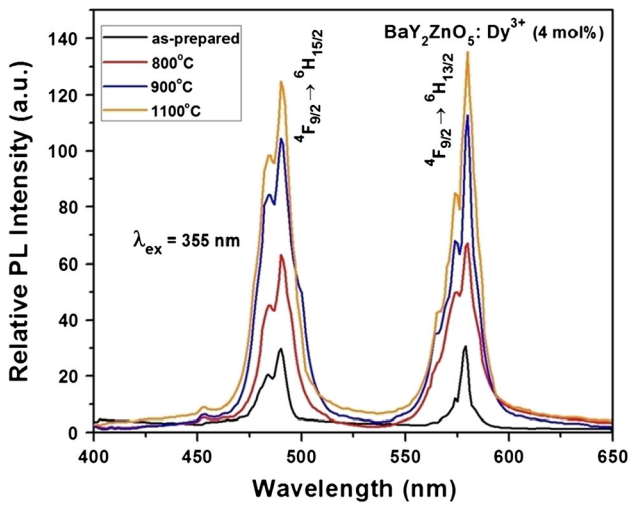

Fig. 6. Photoluminescence (PL) spectra of $BaY_{1.92}Dy_{0.08}ZnO_5$ nanophosphors as-synthesized and sintered at different temperatures, monitored with λ_{ex} = 355 nm.

Table II. Excitation transitions in $BaY_{1.92}Dy_{0.08}ZnO_5$ nanophosphors, sintered at 1100°C, monitored with λ_{em} = 580 nm

Transition	Wavelength (nm)	Transition	Wavelength (nm)
$^6H_{15/2} \rightarrow {}^4K_{13/2} + {}^4H_{13/2}$	300.5	$^6H_{15/2} \rightarrow {}^4I_{13/2}$	388.5
$^6H_{15/2} \rightarrow {}^4K_{15/2}$	327.2	$^6H_{15/2} \rightarrow {}^4M_{21/2}\ {}^4I_{13/2} + {}^4K_{17/2} + {}^4F_{7/2}$	394.5
$^6H_{15/2} \rightarrow {}^4I_{9/2} + {}^4G_{9/2}$	339.2	$^6H_{15/2} \rightarrow {}^4G_{11/2}$	427.8
$^6H_{15/2} \rightarrow {}^4M_{15/2} + {}^6P_{7/2}$	354.5	$^6H_{15/2} \rightarrow {}^4I_{15/2}$	453.2
$^6H_{15/2} \rightarrow {}^4I_{11/2}$	367.8	$^6H_{15/2} \rightarrow {}^4F_{9/2}$	467.8

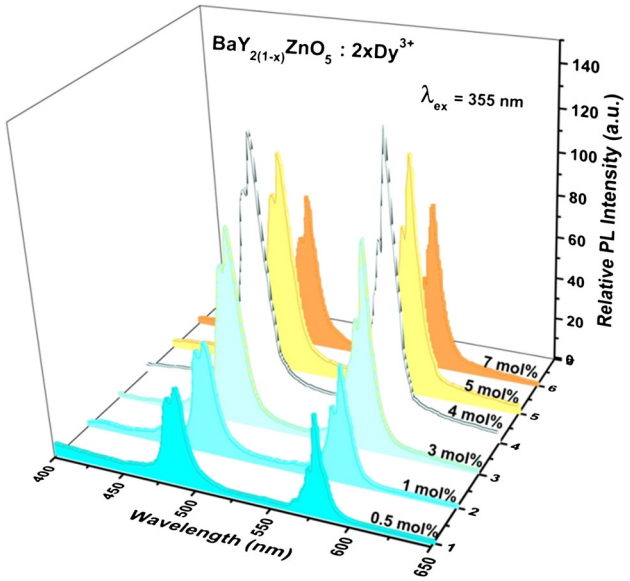

Fig. 7. Photoluminescence (PL) spectra of $BaY_{2(1-x)}Dy_{2x}ZnO_5$ nanophosphors sintered at 1100°C, doped with different amounts of dysprosium, monitored at λ_{ex} = 355 nm.

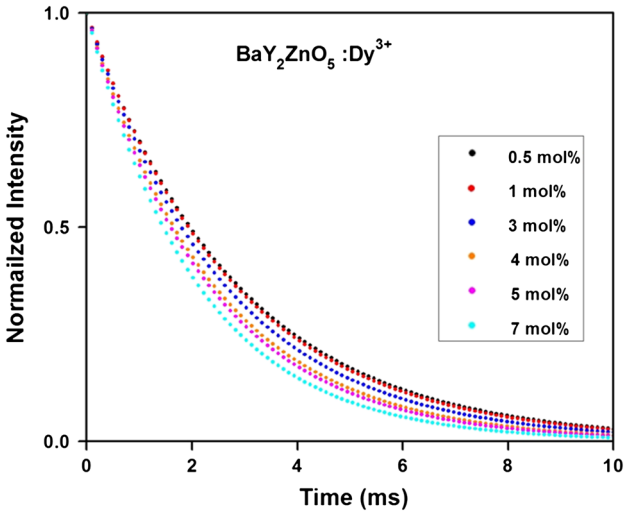

Fig. 8. Luminescence decay curves of $BaY_{2(1-x)}Dy_{2x}ZnO_5$ nanophosphors, sintered at 1100°C, doped with different amounts of dysprosium, measured with λ_{ex} = 355 nm and λ_{em} = 580 nm.

$BaY_{2(1-x)}ZnO_5$ nanophosphors, where x = 0.5–7 mol.%, recorded under excitation at 355 nm ($^6H_{15/2} \rightarrow {}^4M_{15/2} + {}^6P_{7/2}$) are shown in Fig. 8.

All the decay curves were found to obey single exponential behavior, represented by the equation:

$$I = I_0 \exp(-t/\tau) \quad (3)$$

where τ is the radiative decay time, I and I_0 are the luminescence intensities at times t and 0, respectively. Calculated average lifetimes for 0.5, 1, 3, 4, 5, and 7 mol.% Dy^{3+} ions in $BaY_{2(1-x)}ZnO_5$ nanophosphors are 2.84, 2.78, 2.59, 2.38, 2.29, and 2.09 ms, respectively. For $BaY_{2(1-x)}Dy_{2x}ZnO_5$ nanophosphors

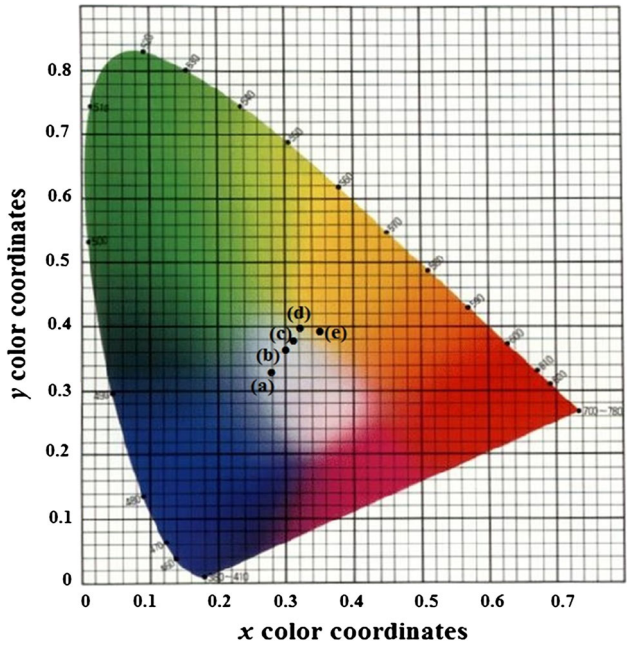

Fig. 9. CIE color (x, y) coordinates for (a) 0.5 mol.%, (b) 1 mol.%, (c) 3 mol.%, (d) 4 mol.%, and (e) 7 mol.% Dy^{3+} ions in BaY_2ZnO_5 nanophosphors sintered at 1100°C after excitation at 355 nm.

lifetimes decrease with increasing dopant concentration, because of non-radiative energy transfer between optically active ions at higher content, owing to the well known concentration quenching mechanism. The Commission International De I'Eclairage (CIE) chromaticity coordinates for $BaY_{2(1-x)}ZnO_5$ nanophosphors doped with 0.5–7 mol.% dysprosium under 355 nm excitation were calculated and are presented in Fig. 9. $BaY_{2(1-x)}Dy_{2x}ZnO_5$ powders have excellent color (x, y) coordinates of (0.279, 0.328), (0.303, 0.365), (0.311, 0.379), (0.323, 0.399), (0.339, 0.396), and (0.345, 0.392) for 0.5, 1, 3, 4, 5, and 7 mol.%, respectively, in the white region, comparable with other standard color systems, for example NTSC (0.3101, 0.3162), PAL/SECAM/HDTV (0.3127, 0.329), ProPhoto/Color Match (0.3457, 0.3585), and CIE white light point (0.33, 0.33).[25] It is quite apparent that $BaY_{2(1-x)}Dy_{2x}ZnO_5$ nanophosphor at low concentration has a cool white color, tending slightly to yellowish at higher concentration. The precise emission color tuning on CIE color coordinates makes $BaY_{2(1-x)}Dy_{2x}ZnO_5$ nanophosphor an ideal optical material for UV-white LED applications.

CONCLUSIONS

BaY_2ZnO_5 nanoparticles doped with different concentrations of dysprosium ions have been synthesized by use of a low-cost, rapid, simple, and environment friendly solution-combustion process. $BaY_{2(1-x)}Dy_{2x}ZnO_5$ nanophosphors have the orthorhombic structure, and the mean particle size ranges from 80 to 90 nm. On excitation at 355 nm,

$BaY_2ZnO_5:Dy^{3+}$ nanoparticles generate white light as a result of blue ($^4F_{9/2} \rightarrow {}^6H_{15/2}$) and yellow ($^4F_{9/2} \rightarrow {}^6H_{13/2}$) emission. The dependence of PL intensity on sintering temperature and dopant content was also studied. Increased PL intensity with sintering temperature may be attributed to better crystallization and reduction of the number of defects, which serve as centers of non-radiative relaxation in nanophosphors. The concentration of dysprosium ions has a significant effect on luminescence intensity and maximum PL was obtained for 4 mol.% Dy^{3+}. Highly optimized luminescence in the white region indicates Dy^{3+}-doped BaY_2ZnO_5 nanophosphor is a promising candidate for advanced display applications.

ACKNOWLEDGEMENTS

One of the authors, Ms. Sonika, gratefully acknowledges financial support in the form of JRF (UGC) New Delhi, India.

REFERENCES

1. A. Bao, H. Yang, and C. Tao, *Curr. Appl. Phys.* 9, 1252 (2009).
2. Sonika, S.D. Han, S.P. Khatkar, M. Kumar, and V.B. Taxak, *Mater. Sci. Eng. B* 178, 1436 (2013).
3. Z. Zhu, D. Liu, H. Liu, G. Li, J. Du, and Z. He, *J. Lumin.* 132, 261 (2012).
4. Y. Zheng, Y. Huang, M. Yang, N. Guo, H. Qaio, Y. Jia, and H. You, *J. Lumin.* 132, 362 (2012).
5. X. Zhang, Z. Zhang, and H.J. Seo, *J. Alloys Compd.* 509, 4875 (2011).
6. R.G.A. Kumar, S. Hata, K.-I. Ikeda, and K.G. Gopchandran, *Ceram. Int.* 40, 2915 (2014).
7. M.J.J. Lammers, H. Donker, and G. Blasse, *Mater. Chem. Phys.* 1313, 527 (1985).
8. C. Guo, J. Yu, J.H. Jeong, Z. Ren, and J. Bai, *Phys. B* 406, 916 (2011).
9. L. Shi and H.J. Seo, *J. Lumin.* 131, 523 (2011).
10. Y. Huang, L. Shi, E.S. Kim, and H.J. Seo, *J. Appl. Phys.* 105, 013512 (2009).
11. B. Tian, B. Chen, Y. Tian, J. Sun, X. Li, J. Zhang, H. Zhang, L. Cheng, and R. Hua, *J. Chem. Phys. Solids* 73, 1314 (2012).
12. C.H. Liang, L.G. Teoh, K.T. Liu, and Y.S. Chang, *J. Alloys Compd.* 517, 9 (2012).
13. C. Guo, X. Ding, and Y. Xu, *J. Am. Ceram. Soc.* 93, 1708 (2010).
14. I. Etchart, I. Hernández, A. Huignard, M. Bérard, M. Laroche, W.P. Gillin, R.J. Curry, and A.K. Cheetham, *J. Mater. Chem.* 21, 1387 (2011).
15. H.Y. Chen, R.Y. Yang, and S.J. Chang, *J. Phys. Chem. Solids* 74, 344 (2013).
16. S. Kunimin and S. Fujihara, *J. Electrochem. Soc.* 157, J175 (2010).
17. H.Y. Chen, R.Y. Yang, and S.J. Chang, *Mater. Lett.* 64, 2548 (2010).
18. S. Singh, S.P. Khatkar, M. Kumar, and V.B. Taxak, *J. Mater. Sci.: Mater. Electron.* 24, 4677 (2013).
19. G.K. Cruz, H.C. Basso, M.C. Terrile, and R.A. Carvalho, *J. Lumin.* 86, 155 (2000).
20. C.H. Liang, Y.C. Chang, and Y.S. Chang, *Appl. Phys. Lett.* 93, 211902 (2008).
21. H.Y. Chen, M.H. Weng, R.Y. Yang, and S.J. Chang, *Ceram. Int.* 37, 1521 (2011).
22. Sonika, S.P. Khatkar, M. Kumar, and V.B. Taxak, *J. Mater. Sci*. 49, 572 (2014).
23. I. Etchart, M. Bérard, M. Laroche, A. Huignard, I. Hernández, W.P. Gillin, R.J. Curry, and A.K. Cheetham, *Chem. Commun.* 47, 6263 (2011).
24. J.A. Kaduk, W. Wong-Ng, W. Greenwood, J. Dillingham, and B.H. Toby, *J. Res. Natl. Inst. Stand. Technol.* 104, 147 (1999).
25. G.S.R. Raju, J.Y. Park, H.C. Jung, B.K. Moon, J.H. Jeong, and J.H. Kim, *Curr. Appl. Phys.* 9, e92 (2009).
26. D. Gao, Y. Li, X. Lai, Y. Wei, J. Bi, Y. Li, and M. Liu, *Mater. Chem. Phys.* 126, 391 (2011).
27. S.D. Han, S.P. Khatkar, V.B. Taxak, G. Sharma, and D. Kumar, *Mater. Sci. Eng. B* 129, 126 (2006).
28. C.R. Kesavulu and C.K. Jayasankar, *Mater. Chem. Phys.* 130, 1078 (2011).
29. S.T. Aruna and A.S. Mukasyan, *Curr. Opin. Solid State Mater. Sci.* 12, 44 (2008).
30. S. Ekambaram and K.C. Patil, *J. Alloys Compd.* 448, 7 (1997).
31. G. Blasse and B.C. Grabmaier, *Luminescent Materials* (Berlin Heidelberg: Springer, 1994).
32. J. Mulak and M. Mulak, *J. Phys. A: Math. Theor.* 40, 2063 (2007).
33. L.A. Diaz-Torres, E.D.L. Rosa, P. Salas, V.H. Romero, and A. Angeles-Chavez, *J. Solid State Chem.* 181, 75 (2008).